when the reversal potential for ions passing through GABA receptor channels is more positive than resting potential. Therefore, we compared, in pacemaker and inhibited cells, resting potential and the reversal potential of synaptic events remaining in the presence of glutamate receptor blockers (Fig. 4, B and C). In pacemaker cells that discharged synchronously with interictal bursts, synaptic events recorded in NBQX and APV reversed at -55 ± 12 mV ($n = 9$), more depolarized ($P < 0.025$; Student's t test) than their resting potential of -67 ± 10 mV ($n = 9$). Synaptic events in inhibited cells, reversed at -72 ± 7 mV ($n = 25$), while the resting potential, -62 ± 8 mV ($n = 25$), was less hyperpolarized ($P < 0.001$). These data show that IPSPs reverse at potentials positive to rest (*24*, *25*) in a subset of subicular neurons.

This in vitro activity corresponds in several respects to interictal activity in mesial temporal lobe epilepsy. Epileptiform bursts were generated in the subiculum but not in other regions, which suggests that they did not result from general defects in slice condition. Interictal activity seems to be generated by a minority of subicular neurons including interneurons and a subset of pyramidal cells (Fig. 3, C and E). Both glutamatergic and GABAergic signaling are involved (Fig. 3, A and B), in line with previous suggestions from work on epileptic human tissue (*8*). Reciprocal interactions between the three cell types may underlie the generation of this activity. The difference between discharging and inhibited pyramidal cells apparently results from different reversal potentials for GABAergic events. GABA-mediated synaptic events may also depolarize interneurons, although we did not test this explicitly.

One feature of the sclerotic hippocampus is the formation of aberrant connections between dentate granule cells (*26*, *27*). Our data suggest that plastic changes also occur in the subiculum. Thus, loss of both postsynaptic (dentate gyrus to CA3) and presynaptic (CA1 to subiculum) cells initiates an epileptogenic plasticity. In the subiculum, the reactive plasticity includes changes in GABAergic signaling. A hyperexcitability in the subiculum would, unlike in the dentate region, permit propagation to other cortical structures. Our observation of depolarizing synaptic GABA responses in some subicular pyramidal cells recalls the GABAergic excitation of early development, which results from delayed expression of the KCC2 transporter (*23*, *24*). Deafferentation may initiate a regressive switch in GABAergic response polarity from hyperpolarizing to depolarizing (*25*), perhaps in the most severely denervated cells. Understanding changes in the subiculum (*4*, *25*) induced by the loss of excitatory inputs from CA1 cells may eventually provide therapeutic avenues for preventing seizure development after hippocampal insults.

References and Notes

1. D. V. Lewis, *Curr. Opin. Neurol.* **12**, 197 (1999).
2. M. Dichter, W. A. Spencer, *J. Neurophysiol.* **32**, 649 (1969).
3. R. K. S. Wong, R. D. Traub, *J. Neurophysiol.* **49**, 442 (1983).
4. R. A. McKinney *et al.*, *Nature Med.* **3**, 990 (1997).
5. P. Salin *et al.*, *J. Neurosci.* **15**, 8234 (1995).
6. R. S. Fisher, *Brain Res. Rev.* **14**, 245 (1989).
7. B. W. Colder *et al.*, *J. Neurophysiol.* **75**, 2496 (1996).
8. R. Kohling *et al.*, *Brain* **121**, 1073 (1998).
9. P. A Schwartzkroin *et al.*, *Ann. Neurol.* **13**, 249 (1983).
10. P. A. Schwartzkroin, M. M. Haglund, *Epilepsia* **27**, 523 (1986).
11. Patients were between 22 and 54 years old and had suffered from pharmacoresistant focal seizures for 25 years on average. Seizure frequency was 11 ± 10 (mean $\pm$ SD) per month. Functional imaging, morphological studies, and inspection of slices revealed a hippocampal sclerosis of variable severity. Surface EEG recordings were obtained from all patients, and intracranial recordings were obtained from hippocampal structures in four cases.
12. S. Lehericy *et al.*, *Neuroradiology* **39**, 788 (1997).
13. J. Engel Jr., *Curr. Opin. Neurol.* **7**, 140 (1994).
14. Portions of mesial temporal lobe, obtained from the neurosurgeon, with the patients' informed consent, were immediately immersed in 26 mM $NaHCO_3$, 1 mM KCl, 10 mM $MgCl_2$, 1 mM $CaCl_2$, 248 mM sucrose, and 10 mM glucose equilibrated with 5% CO_2 in 95% O_2 at 4°C. Hippocampal-subicular slices 400 μm thick were prepared with a vibratome in the same solution and transferred to a recording chamber. They were maintained at 35° to 37°C, perfused with 124 mM NaCl, 26 mM $NaHCO_3$, 4 mM KCl, 2 mM $MgCl_2$, 2 mM $CaCl_2$, and 10 mM glucose and equilibrated with 5% CO_2 in 95% O_2. The time between tissue reception and slice preparation was typically 45 min.
15. Intracellular records were made with 2 M KAc-filled glass microelectrodes and extracellular signals were recorded with etched tungsten wires as described in [I. Cohen, R. Miles, *J. Physiol. (London)* **524**, 485 (2000)].
16. F. H. Lopes da Silva, M. P. Witter, P. H Boeijinga, A. H. Lohman, *Physiol. Rev.* **70**, 453 (1990).
17. Fast excitatory postsynaptic potentials were blocked with 5 μM NBQX or 20 μM CNQX and 100 μM APV. $GABA_A$ receptor-mediated IPSPs were suppressed by picrotoxin (50 μM), bicuculline (10 μM), or gabazine (SR-95531; 5 μM).
18. J. R. Greene, S. Totterdell, *J. Comp. Neurol.* **380**, 395 (1997).
19. M. Stewart, R. K. S. Wong, *J. Neurophysiol.* **70**, 232 (1993).
20. P. Parra, A. I. Gulyas, R. Miles, *Neuron* **20**, 983 (1998).
21. D. A. Prince, B. J. Wilder, *Arch. Neurol.* **16**, 194 (1967).
22. I. Cohen *et al.*, unpublished data ($n = 49$).
23. Y. Ben-Ari, E. Cherubini, R. Corradetti, J. L. Gaiarsa, *J. Physiol. (London)* **416**, 303 (1989).
24. C. Rivera *et al.*, *Nature* **397**, 251 (1999).
25. C. Vale, D. H. Sanes, *J. Neurosci.* **20**, 1912 (2000).
26. T. Sutula *et al.*, *J. Comp. Neurol.* **390**, 578 (1998).
27. P. R. Patrylo, F. E. Dudek, *J. Neurophysiol.* **79**, 418 (1998).

28. We thank P. Parra, D. Fricker, R. Traub, H. Korn, and F. Gabbiani for help and comments on the manuscript. Supported by INSERM, Fondation Française pour la Recherche sur L'Epilepsie, NIH (MH54671), CNRS, and Fondation pour la Recherche Médicale.

24 July 2002; accepted 4 October 2002

Transition State Stabilization by a Catalytic RNA

Peter B. Rupert,[1] Archna P. Massey,[2] Snorri Th. Sigurdsson,[2] Adrian R. Ferré-D'Amaré[1]*

The hairpin ribozyme catalyzes sequence-specific cleavage of RNA through transesterification of the scissile phosphate. Vanadate has previously been used as a transition state mimic of protein enzymes that catalyze the same reaction. Comparison of the 2.2 angstrom resolution structure of a vanadate–hairpin ribozyme complex with structures of precursor and product complexes reveals a rigid active site that makes more hydrogen bonds to the transition state than to the precursor or product. Because of the paucity of RNA functional groups capable of general acid-base or electrostatic catalysis, transition state stabilization is likely to be an important catalytic strategy for ribozymes.

The hairpin ribozyme catalyzes reversible, site-specific cleavage of the phosphodiester backbone of RNA through transesterification (*1*) (Fig. 1A). The ribozyme is fully active in vitro when the physiologic counterion Mg^{2+} is replaced with cobalt (III) hexammine (*2*–*4*). This complex ion mimics hydrated Mg^{2+} but cannot directly coordinate or activate water or RNA ligands. Therefore, nucleic acid moieties alone must be responsible for promoting cleavage 10^6 times faster than the background rate.

A crystal structure of a hairpin ribozyme bound to an inhibitor RNA has been reported (*5*). The minor grooves of two irregular helices, stems A and B, dock to form the active site. One of the strands of stem A contains the scissile phosphate (Fig. 1B). In the crystal structure, the nucleotides flanking this phosphate are splayed apart (Fig. 1C), aligning the 2′-OH nucleophile (blocked with a methyl group to prevent cleavage) with the reactive phosphorus and the 5′-oxo leaving group. The in-line conformation (required for the second-order nucleophilic substitution transesterification) and biochemical and biophys-

[1]Division of Basic Sciences, Fred Hutchinson Cancer Research Center, 1100 Fairview Avenue North, Seattle, WA 98109–1024, USA. [2]Department of Chemistry, University of Washington, Box 351700, Seattle, WA 98195–1700, USA.

*To whom correspondence should be addressed. E-mail: aferre@fhcrc.org

ical data suggested that the ribozyme-inhibitor cocrystal structure represents the ground state, or precursor, conformation (*5*).

To further our understanding of this ribozyme's catalytic mechanism, we have now determined its structure in complex with a transition state mimic at 2.2 Å resolution (Table 1). We crystallized a hairpin ribozyme construct missing the scissile phosphate (Fig. 1B) in the presence of vanadate (*6*) (fig. S1). The electron density feature present in the active site can be assigned to vanadate based on its size, shape, and anomalous scattering (Fig. 1, C and D). Vanadate has previously been used in crystallographic studies of ribonuclease A, a protein enzyme that catalyzes the same reaction as the hairpin ribozyme (*7*, *8*). The transesterification reaction proceeds through a trigonal bipyramidal, pentacoordinate phosphorus transition state. Although the vanadate geometry is that of a distorted trigonal bipyramid (*6*), it is pentacoordinate and an approximate mimic of the transition state that is otherwise impossible to visualize experimentally. How accurately vanadate mimics the transition state of ribonuclease A remains a topic of active research (*9*–*14*).

In order to mimic the transition state of the hairpin ribozyme, vanadate must directly coordinate three RNA ligands: the 2′- and 3′-oxygens of nucleotide –1 and the 5′-oxygen of nucleotide +1 (Fig. 1B). Three lines of evidence suggest that the vanadate present in the active site is indeed a transition state mimic.

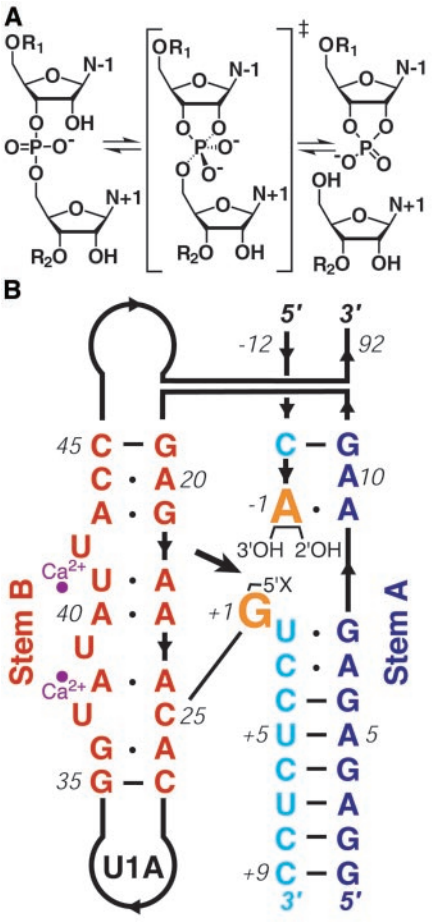

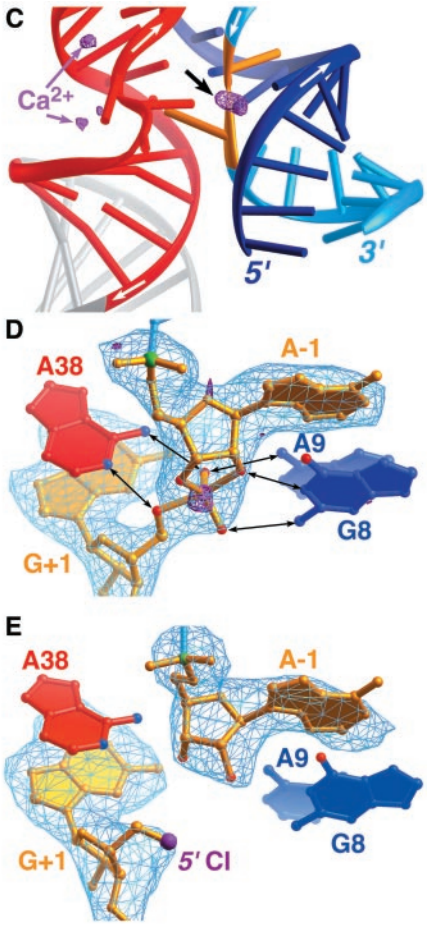

Fig. 1. Characterization of the vanadate-hairpin ribozyme complex. (**A**) Schematic of the reversible transesterification reaction catalyzed by the hairpin ribozyme. The concerted reaction (*36*) proceeds through a pentacoordinate trigonal bipyramidal phosphorus transition state (‡). (**B**) Sequence of the crystallization construct, numbered following convention. The ribozyme strand consists of 92 nucleotides (nt). The substrate strand (light blue, in stem A) is split (big arrow) into oligonucleotides of 12 and 9 nt, and the scissile phosphate deleted. The 5′ function of the 9 nt RNA (5′X) is either hydroxyl or chlorine. Thick lines with arrows denote chain direction; thin lines, Watson-Crick pairs; and dots, noncanonical pairs. The ribozyme contains an U1A protein binding site used for crystallization (*6*). (**C**) Schematic of the active site of the vanadate complex with anomalous difference map features (purple mesh). The nucleotides flanking the active site (yellow) are splayed apart. The map was calculated with CuK_α x-ray data (*6*) and contoured at 3.5 standard deviations above mean peak height (SD). The strongest features correspond to the active site vanadate (black arrow, at 6 SD the highest peak in the map) and two Ca^{2+} ions (purple arrows, 4.5 and 4.0 SD). White arrows denote 5′ to 3′ RNA chain direction. (**D**) Omit $|F_o| - |F_c|$ map (*6*) (where F_o and F_c are the observed and calculated structure factors, respectively) of the active site of the vanadate complex contoured at 3 SD (blue mesh) superimposed on the refined crystallographic model. The anomalous difference feature (purple mesh, 2.5 SD, from 1.0 Å wavelength x-ray data) is coincident with the vanadium atom. Selected hydrogen bonds are shown (black double-headed arrows). (**E**) Omit $|F_o| - |F_c|$ map (3 SD) of the active site of the ribozyme with the 5′-chloro substrate crystallized in the presence of vanadate. Note the absence of vanadate electron density.

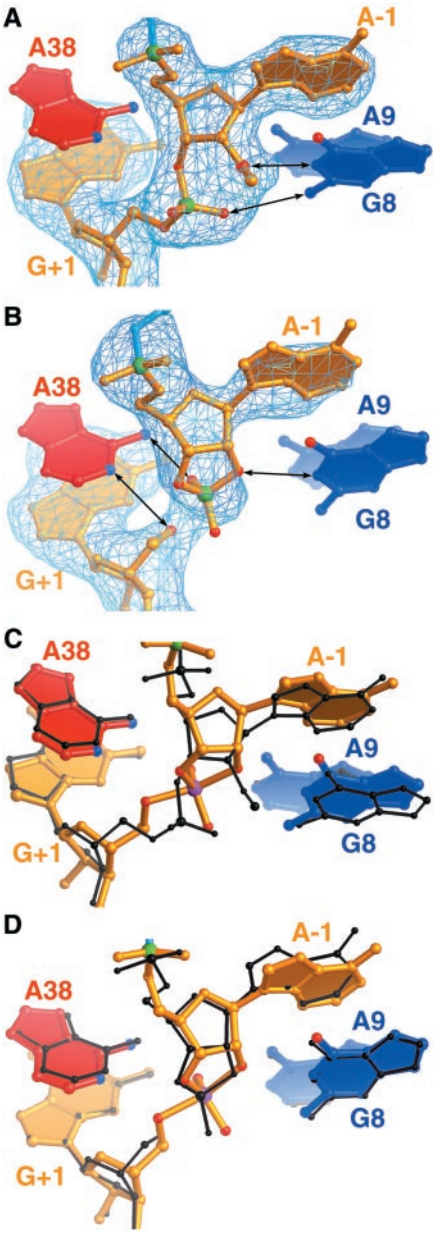

Fig. 2. Comparison of the active sites of precursor, transition state mimic, and product structures. (**A**) Omit $|F_o| - |F_c|$ map (3 SD) of the precursor, trapped by replacing the 2′-OH nucleophile with a methoxy group (*5*). Arrows and mesh are as in Fig. 1. (**B**) Omit $|F_o| - |F_c|$ map (3 SD) of the ribozyme-product complex. (**C**) Superposition of the precursor (black) and vanadate models. (**D**) Superposition of product (black) and vanadate models. Within experimental error (Table 1), the active site is rigid (*16*).

First, the space available in the active site of the ribozyme precludes the simultaneous presence of the three RNA oxygen ligands and a fully hydrated vanadate ion with five oxygens. Second, whereas vanadate electron density is present in the active site, it is absent near the terminal 2′,3′-diols of the RNA (Fig. 1C and fig. S2). This implies that coordination by two RNA oxygens is not enough to bind the vanadate anion to the anionic nucleic acid. In contrast, the three RNA oxygens in the active site bind vanadate. Third, to test definitively the importance of the third active site oxygen ligand for vanadate binding, we synthesized a hairpin ribozyme construct in which the active site 5′-OH was replaced with a chlorine (Fig. 1B and fig. S3) (*15*), and we crystallized it in the presence of vanadate. Replacement of a single active site RNA hydroxyl group with chlorine abolishes the active site electron density feature (Fig. 1E) and eliminates the vanadate anomalous difference peak (not shown). This demonstrates that even in the active site, the 2′,3′-diol is not sufficient for vanadate binding. Therefore, the vanadate bound in the active site (Fig. 1D) must coordinate all three RNA oxygen ligands.

In addition to the precursor structure (Fig. 2A), we have determined the structure of a hairpin ribozyme bound to an all-RNA substrate (Table 1). Because the ribozyme catalyzes both the cleavage reaction and the reverse ligation, the electron density consists of a mixture of the cleaved and ligated substrate (Fig. 2B). The cleaved form, with a 2′,3′-cyclic phosphate, predominates over the precursor in these crystals (*6*). Superposition of the precursor, transition state mimic, and product structures (Fig. 2, C and D) demonstrates that the active site of the ribozyme is essentially rigid (*16*), with motion confined to the scissile phosphate and the ribose of nucleotide –1. This ribose undergoes a change in puckering as its 2′-oxygen attacks the phosphate and the five-membered ring of the 2′,3′-cyclic phosphate is formed.

Comparison of the number of hydrogen bonds (*6*) in the hairpin ribozyme active site between the substrate analog, transition state mimic, and product complexes (Fig. 3 and table S1) suggests that this catalytic RNA binds most tightly to the transition state (*17*). In the precursor, the ribozyme uses the nucleobase of G8 to make two hydrogen bonds: one to the 2′-OH nucleophile and one to a phosphate oxygen (Figs. 2A and 3A). In the transition state mimic, five hydrogen bonds are formed between the nucleobases of G8, A9, and A38 in the active site and vanadate oxygens (Figs. 1D and 3B). In the product, the nucleobases of G8 and A38 make two hydrogen bonds to the cyclic phosphate and one bond to the 5′-OH leaving group (Figs. 2B and 3C).

Previous biochemical experiments have implicated A9, A10, A38, and G8 in catalysis. Free nucleotides do not have functional groups that ionize near neutral pH (*18*), although they can have perturbed acidities as part of intricately folded ribozymes (*19*, *20*). Because of the principle of microscopic reversibility, if an RNA functional group is to act as a general acid catalyst in the concerted cleavage reaction, then it must also function as a general base in ligation. Thus, unless their pK_a (where K_a is the acid constant) are shifted to near-neutrality, hairpin ribozyme nucleotides will not be effective general acid-base catalysts.

Analysis of the catalytic role of G8 with the use of purine analogs demonstrated that the rate of the cleavage reaction is greatest when the N1 imino nitrogen of the purine at position 8 is protonated (*21*). Our structures show that this functional group is a hydrogen bond donor to the 2′-oxygen of nucleotide –1 in the precursor, transition state,

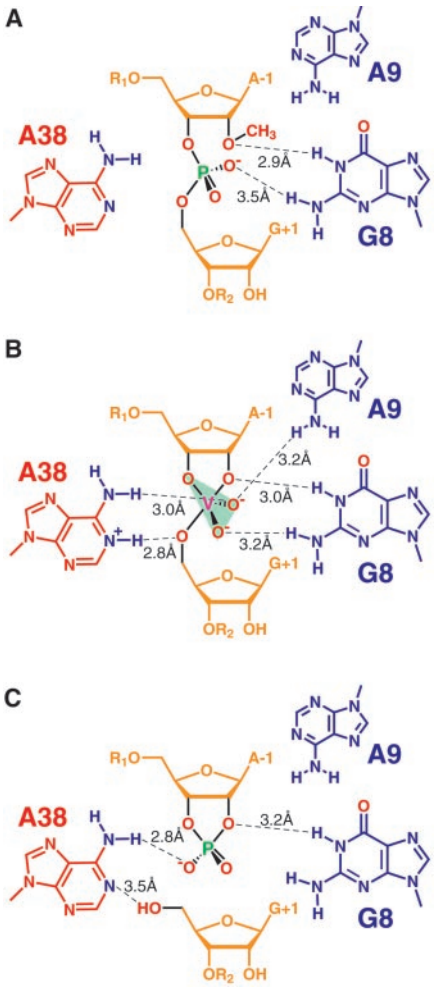

Fig. 3. Summary of active site hydrogen bonds (*6*). (**A**) Precursor complex stabilized by two hydrogen bonds (dashed lines) from G8. (**B**) Transition state mimic complex stabilized by five hydrogen bonds. (The green triangle connects the equatorial oxygens of the vanadate.) Although modification interference studies found no evidence that N1 of A38 is protonated (*25*), full time courses were not examined by those authors. Protonation is inferred from the distance between N1 of A38 and the 5′-oxygen (*6*). (**C**) Product complex stabilized by three hydrogen bonds. The hydrogen bond between N1 of A38 and the 5′-OH of G+1 would orient the latter for the ligation reaction.

Table 1. Crystallographic statistics. Details of the crystallization conditions and structure determinations are provided in the supporting online material (*6*). The headings Methoxy, Vanadate, and All-RNA refer to the substrate mimic, transition state mimic, and product complexes, respectively; 5′-Chloro refers to the ribozyme with the 5′-chloro 9 nt substrate crystallized in the presence of vanadate (Fig. 1E). Precursor complex statistics (Methoxy) reflect further refinement of the reported (*5*) structure. Reflections/redundancy: reflections are the number of unique reflections; redundancy is the total number of observations divided by the number of unique reflections. R_{sym} is defined as $\Sigma|I - \langle I\rangle|/\Sigma I$, where I is the observed intensity and $\langle I\rangle$ is the statistically weighted absolute intensity of multiple measurements of symmetry related reflections. In this row and the two that follow, values in parentheses correspond to the highest resolution shells. R_{work} is defined as $100 \times \Sigma|F_o - F_c|/\Sigma|F_c|$. R_{free} is the same as R_{work}, but calculated with a random 10% of the data excluded from refinement. Rmsd, root mean square differences of model bond lengths and angles from ideal geometry. $\langle B\rangle$ active site, mean B factors for all atoms in the active site core [defined in (*6*)]. Coordinate error, cross-validated σA mean coordinate error (*37*).

	Methoxy	Vanadate	All-RNA	5′-Chloro
	Diffraction data			
Resolution (Å)	100–2.4	20–2.2	30–2.4	30–2.6
Reflections/redundancy	41290/3.6	57275/3.6	43840/3.6	34446/3.3
R_{sym} (%)	6.7 (26.1)	6.4 (48.9)	6.6 (26.5)	6.6 (60.8)
$\langle I\rangle/\langle\sigma(I)\rangle$	22.8 (2.1)	22.9 (1.9)	24.7 (3.1)	22.0 (1.7)
Completeness (%)	95.6 (73.9)	99.6 (99.0)	97.7 (81.7)	98.8 (96.4)
	Refinement			
Atoms total/water/ion	6478/103/35	6572/198/37	6634/237/34	6383/45/26
R_{work}/R_{free}	22.9/28.5	23.0/26.5	22.1/26.5	22.3/28.0
Rmsd lengths (Å)/angles (°)	0.006/1.20	0.006/1.18	0.005/1.12	0.006/1.22
$\langle B\rangle$ active site (Å^2)	81.7	77.3	74.1	89.3
Coordinate error (Å)	0.44	0.47	0.32	0.57

and product (Fig. 3). Protonation would be consistent with a structural role as an obligate hydrogen bond donor, rather than an acid-base catalyst (*22*). Presumably, proton transfer to and from the 2′-oxygen of nucleotide –1 is carried out by water. Investigation of the importance of the nucleobases of G8, A9, and A10 using abasic ribozyme constructs showed that individually, these purines contribute surprisingly little to catalytic rate enhancement (*23*), consistent with a role in binding or ribozyme architecture rather than general acid-base catalysis. Examination of the effect of adenosine base ionization on hairpin ribozyme activity with the use of nucleotide analog interference mapping (*24*) demonstrated that all pH-dependent interferences are due to structural destabilization of the RNA (*25*, *26*). Our transition state mimic and product structures (Fig. 3, B and C) suggest that N1 of A38 could have a perturbed pK_a, and this functional group could also play a role in protonating the leaving group during the cleavage reaction.

Pauling proposed in 1946 that enzymes could function by binding more tightly to the transition state than to the ground states, thus lowering the activation energy (*27*). The structural analysis presented here shows that the hairpin ribozyme has evolved to maximize its hydrogen bonding interactions with the trigonal bipyramidal transition state (Fig. 3) (*28*). For some protein enzymes, catalysis is known to result exclusively from binding energy (*29*). Like other RNA catalysts (*30*, *31*), the hairpin ribozyme also uses the binding energy of groups distant to the active site to accelerate its reaction: docking of stems A and B leads to a folding transition (*5*, *32*, *33*) that aligns the substrate within a rigid (*16*) active site. Precise positioning of substrate can effect large rate enhancements (*34*). Recent work on other catalytic RNAs, such as the ribosome (*35*), suggests that the combination of transition state stabilization and precise substrate positioning used by the hairpin ribozyme may be a catalytic strategy frequently used by RNA enzymes.

References and Notes

1. M. J. Fedor, *J. Mol. Biol.* **297**, 269 (2000).
2. A. Hampel, J. A. Cowan, *Chem. Biol.* **4**, 513 (1997).
3. K. J. Young, F. Gill, J. A. Grasby, *Nucleic Acids Res.* **25**, 3760 (1997).
4. S. Nesbitt, L. A. Hegg, M. J. Fedor, *Chem. Biol.* **4**, 619 (1997).
5. P. B. Rupert, A. R. Ferré-D'Amaré, *Nature* **410**, 780 (2001).
6. Materials and Methods are available as supporting online material on *Science* Online.
7. A. Wlodawer, M. Miller, L. Sjolin, *Proc. Natl. Acad. Sci. U.S.A.* **80**, 3628 (1983).
8. B. D. Wladkowski, L. A. Svensson, L. Sjolin, J. E. Ladner, G. L. Gilliland, *J. Am. Chem. Soc.* **120**, 5488 (1998).
9. R. N. Lindquist, J. L. Lynn Jr., G. E. Lienhard, *J. Am. Chem. Soc.* **95**, 8762 (1973).
10. M. Krauss, H. Basch, *J. Am. Chem. Soc.* **114**, 3630 (1992).
11. T. D. Veenstra, L. Lee, *Biophys. J.* **67**, 331 (1994).
12. H. Deng, J. W. Burgner, R. H. Callender, *J. Am. Chem. Soc.* **120**, 4717 (1998).
13. R. T. Raines, *Chem. Rev.* **98**, 1045 (1998).
14. J. M. Messmore, R. T. Raines, *J. Am. Chem. Soc.* **122**, 9911 (2000).
15. A. P. Massey, S. Th. Sigurdsson, in preparation.
16. All-atom superposition of the nucleobases of G8, A9, and A38 (31 atoms) gives root mean square (rms) differences of 0.32 Å and 0.31 Å for the precursor versus the transition state mimic, and the transition state mimic versus the product, respectively.
17. S. O. Shan, D. Herschlag, *Methods Enzymol.* **308**, 246 (1999).
18. W. Saenger, *Principles of Nucleic Acid Structure* (Springer-Verlag, New York, 1984), pp. 107–110.
19. A. T. Perrotta, I. Shih, M. D. Been, *Science* **286**, 123 (1999).
20. S. Nakano, D. M. Chadalavada, P. C. Bevilacqua, *Science* **287**, 1493 (2000).
21. R. Pinard *et al.*, *EMBO J.* **20**, 6434 (2001).
22. It has also been shown that deletion or methylation of the exocyclic amino group of G8 is deleterious for catalysis (*1*, *21*, *24*). This functional group hydrogen bonds to a nonbridging phosphate oxygen in both the precursor and the transition state (Figs. 1D, 2A, and 3).
23. L. L. Lebruska, I. I. Kuzmine, M. J. Fedor, *Chem. Biol.* **9**, 465 (2002).
24. S. P. Ryder, S. A. Strobel, *Nucleic Acids Res.* **30**, 1287 (2002).
25. S. P. Ryder *et al.*, *RNA* **7**, 1454 (2001).
26. When examined with the use of a stable RNA construct, the only adenosine functional group that interferes with ribozyme activity is the exocyclic amine of A38, and this interference is independent of pH (*25*). In both transition state and product, this amine donates a hydrogen bond to a nonbridging phosphate oxygen (Figs. 1D, 2A, and 3). In a destabilized construct, the exocyclic amine of A9 shows a pH-independent interference (*25*). This can be explained by the hydrogen bond it makes to the transition state (Figs. 1D and 3B).
27. L. Pauling, *Chem. Eng. News* **24**, 1375 (1946).
28. The ribozyme may also destabilize the precursor by desolvating the scissile phosphate and not saturating the partially buried anion with hydrogen bonds.
29. A. Fersht, *Structure and Mechanism in Protein Science* (Freeman and Co., New York, 1999), pp. 420–450.
30. G. J. Narlikar, V. Gopalakrishnan, T. S. McConnell, N. Usman, D. Herschlag, *Proc. Natl. Acad. Sci. U.S.A.* **92**, 3668 (1995).
31. K. J. Hertel, A. Peracchi, O. C. Uhlenbeck, D. Herschlag, *Proc. Natl. Acad. Sci. U.S.A.* **94**, 8497 (1997).
32. Z. Cai, I. J. Tinoco, *Biochemistry* **35**, 6026 (1996).
33. S. E. Butcher, F. H. Allain, J. Feigon, *Nature Struct. Biol.* **6**, 212 (1999).
34. M. I. Page, W. P. Jencks, *Proc. Natl. Acad. Sci. U.S.A.* **68**, 1678 (1971).
35. V. Ramakrishnan, *Cell* **108**, 557 (2002).
36. H. van Tol, J. M. Buzayan, P. A. Feldstein, F. Eckstein, G. Bruening, *Nucleic Acids. Res.* **18**, 1971 (1990).
37. A. T. Brünger *et al.*, *Acta Crystallogr.* **D54**, 905 (1998).

38. We thank the staff of beamlines 5.0.1 and 5.0.2 of the Advanced Light Source (ALS), Lawrence Berkeley National Laboratory, for data collection support; J. Bolduc, P. Heath, and B. Shen for crystallographic and computational support; P. Gafken for mass spectrometry; and J. Simon, B. Stoddard, and G. Varani for discussions. This work was supported by the NIH (grants GM63576 and RR15943 to A.R.F. and GM56947 to S.Th.S.). P.B.R. is a postdoctoral trainee of the Chromosome Metabolism and Cancer training grant from the National Cancer Institute to the Fred Hutchinson Cancer Research Center (FHCRC). Access to ALS beamlines 5.0.1 and 5.0.2 as part of the principal research consortium was funded by general support from the FHCRC. A.R.F. is a Rita Allen Foundation Scholar. Coordinates and structure factors have been deposited with the Protein Data Bank (accession codes 1M5K, 1M5O, 1M5V, and 1M5P for the methoxy, vanadate, all-RNA, and 5′-chloro structures, respectively).

Supporting Online Material

www.sciencemag.org/cgi/content/full/1076093/DC1
Materials and Methods
Figs. S1 to S4
Table S1

12 July 2002; accepted 16 September 2002
Published online 10 October 2002;
10.1126/science.1076093
Include this information when citing this paper.

Critical Roles of Activation-Induced Cytidine Deaminase in the Homeostasis of Gut Flora

Sidonia Fagarasan,[1,2]* Masamichi Muramatsu,[1]* Keiichiro Suzuki,[1] Hitoshi Nagaoka,[1] Hiroshi Hiai,[3] Tasuku Honjo[1]†

Activation-induced cytidine deaminase (AID) plays an essential role in class switch recombination (CSR) and somatic hypermutation (SHM) of immunoglobulin genes. We report here that deficiency in AID results in the development of hyperplasia of isolated lymphoid follicles (ILFs) associated with a 100-fold expansion of anaerobic flora in the small intestine. Reduction of bacterial flora by antibiotic treatment of AID$^{-/-}$ mice abolished ILF hyperplasia as well as the germinal center enlargement seen in secondary lymphoid tissues. Because an inability to switch to immunoglobulin A on its own does not lead to a similar phenotype, these results suggest that SHM of ILF B cells plays a critical role in regulating intestinal microflora.

Colonization of the intestine with microflora is essential for the normal development of humoral and cellular immune responses (*1*, *2*). Intestinal B cells are evolutionarily tailored largely for production of immunoglobulin A (IgA), which is transported across the epithelium into the gut lumen, where it serves as a first line of defense against viral and bacterial pathogens (*3*). It has been long recognized that a